biophysica

MDPI

Article

Transient Slope: A Metric for Assessing Heterogeneity from the Dielectrophoresis Spectrum

Emmanuel Egun [1,2], Tia Wilson [2,3], Zuri A. Rashad [1,2], Rominna Valentine [1,2] and Tayloria N. G. Adams [1,2,3,4,5,*]

[1] Department of Chemical and Biomolecular Engineering, University of California Irvine, Irvine, CA 92697, USA; eegun@uci.edu (E.E.); zrashad@uci.edu (Z.A.R.)
[2] Sue and Bill Gross Stem Cell Research Center, University of California, Irvine, CA 92697, USA; tiaw1@uci.edu
[3] Department of Materials Science Engineering, University of California, Irvine, CA 92697, USA
[4] Department of Biomedical Engineering, University of California, Irvine, CA 92697, USA
[5] Department of Anatomy and Neurobiology, University of California, Irvine, CA 92697, USA
* Correspondence: tayloria@uci.edu

Abstract: Cellular heterogeneity, an inherent feature of biological systems, plays a critical role in processes such as development, immune response, and disease progression. Human mesenchymal stem cells (hMSCs) exemplify this heterogeneity due to their multi-lineage differentiation potential. However, their inherent variability complicates clinical use, and there is no universally accepted method for detecting and quantifying cell population heterogeneity. Dielectrophoresis (DEP) has emerged as a powerful electrokinetic technique for characterizing and manipulating cells based on their dielectric properties, offering label-free analysis capabilities. Quantitative information from the DEP spectrum, such as transient slope, measure cells' transition between negative and positive DEP behaviors. In this study, we employed DEP to estimate transient slope of various cell populations, including relatively homogeneous HEK-293 cells, heterogeneous hMSCs, and cancer cells (PC3 and DU145). Our analysis encompassed hMSCs derived from bone marrow, adipose, and umbilical cord tissue, to capture tissue-specific heterogeneity. Transient slope was assessed using two methods, involving linear trendline fitting to different low-frequency regions of the DEP spectrum. We found that transient slope serves as a reliable indicator of cell population heterogeneity, with more heterogeneous populations exhibiting lower transient slopes and higher standard deviations. Validation using cell morphology, size, and stemness further supported the utility of transient slope as a heterogeneity metric. This label-free approach holds promise for advancing cell sorting, biomanufacturing, and personalized medicine.

Keywords: heterogeneity; dielectrophoresis; dielectrophoresis spectrum; transient slope; label-free cell analysis; mesenchymal stem cells; cancer cells

Citation: Egun, E.; Wilson, T.; Rashad, Z.A.; Valentine, R.; Adams, T.N.G. Transient Slope: A Metric for Assessing Heterogeneity from the Dielectrophoresis Spectrum. *Biophysica* **2024**, *4*, 695–710. https://doi.org/10.3390/biophysica4040045

Academic Editor: Attila Borics

Received: 18 November 2024
Revised: 8 December 2024
Accepted: 13 December 2024
Published: 14 December 2024

1. Introduction

Cellular heterogeneity is an intrinsic property of biological systems that manifests at multiple levels, ranging from individual cells to entire tissues [1]. This variability arises from genetic, epigenetic, and environmental factors, leading to diverse cell functions within a population [2]. Heterogeneity plays a crucial role in various biological processes, such as human development, immune response, and disease progression [3]. The ability to measure and characterize cellular heterogeneity is essential in understanding complex biological phenomena such as cell differentiation, optimizing cell sorting and biomanufacturing processes, and improving treatment outcomes in personalized medicine. However, despite its significance, quantifying cell population heterogeneity remains challenging due to the lack of universally accepted markers.

Human mesenchymal stem cells (hMSCs) are a prime example of a heterogeneous cell population. HMSCs are multipotent cells that can differentiate into various lineages, including osteoblasts, adipocytes, and chondrocytes [4]. They are widely studied for

their potential in regenerative medicine and tissue engineering. For example, hMSCs are frequently used to repair bone defects, particularly in cases of non-union bone fractures or large bone defects where traditional healing is insufficient [5]. Additionally, hMSCs play a role in modulating immune responses by secreting anti-inflammatory cytokines and inhibiting T-cell proliferation, making them promising for treating immune-related disorders [6]. However, the inherent heterogeneity within hMSC populations complicates their clinical applications. Variations in cell size, morphology, differentiation potential, and surface marker expression contribute to differences in their therapeutic efficacy [7]. Therefore, understanding and characterizing cell population heterogeneity is essential in optimizing hMSC-based therapies, as it can impact their ability to repair tissues and modulate immune responses.

Dielectrophoresis (DEP) has emerged as a promising technique for analyzing and addressing challenges associated with heterogeneity by characterizing and manipulating cell populations based on their dielectric properties. By leveraging the differences in dielectric properties of cell subpopulations, DEP can manipulate and sort cells based on variations in their cell membrane and cytoplasm without the need for labels [8]. In the context of hMSCs, DEP analysis offers potential for selecting specific subpopulations of cells and refining cell population heterogeneity. For instance, Song et al. enriched osteoblasts from a mixture of differentiated and undifferentiated hMSCs, demonstrating that DEP can yield reasonably pure, homogeneous subpopulations [9]. Similarly, Yoshioka et al. achieved good purity when enriching immortalized hMSCs from a mixture of hMSCs and HL-60 cells [10].

Fundamentally, DEP involves the polarization of cells using nonuniform electric fields, causing cell movement that is dependent on their inherent dielectric properties. The key principle is that cells experience a force based on the gradient of the nonuniform electric field, with the direction of the force depending on the relative polarizability of the cell and the surrounding medium [11]. The DEP force, F_{DEP}, is described by [11],

$$F_{DEP} = 2\pi r^3 \varepsilon_m Re[K(\omega)] \nabla \mid E \mid^2, \quad (1)$$

where r is the radius of the cell, ε_m is the permittivity of the surrounding medium, $Re[K(\omega)]$ is the real part of the Clausius–Mossotti factor, which depends on frequency, ω, and $\nabla \mid E \mid^2$ is the gradient of the squared magnitude of the electric field. The Clausius–Mossotti factor is given by [11]

$$K(\omega) = \varepsilon^*_{cell} - \varepsilon^*_m / \varepsilon^*_{cell} + 2\varepsilon^*_m \quad (2)$$

where ε^*_{cell} is the complex permittivity of the cell and ε^*_m is the complex permittivity of the medium. These equations show that the DEP force depends on cell size, dielectric properties of the suspending medium and cell, and spatial variations of the nonuniform electric field.

The movement of cells with DEP is categorized as positive or negative DEP, where cells move toward areas where the nonuniform electric field gradient is strongest (positive DEP) or weakest (negative DEP). By measuring the DEP response at varying frequencies, a DEP spectrum can be generated for a cell population, providing valuable insights into cellular composition and heterogeneity through positive and negative DEP behaviors. Quantitative information can be obtained from the DEP spectrum, such as membrane capacitance [12,13], cytoplasm conductivity [12,13], as well as the transient behavior of cells. One approach to examining the transient behavior is by analyzing the slope of the low-frequency region of the DEP spectrum. The transient slope, assessed using principles from signal processing, has previously been used to characterize neural stem and progenitor cells, astrocytes, neurons, hMSCs, red blood cells, and polystyrene beads [13–15]. By analyzing the DEP spectrum, transient slope emerges as a reliable, label-free metric for detecting cellular heterogeneity, representing the transition of cells from negative to positive DEP behavior [13].

In this study, we used DEP and estimated the transient slope of homogeneous and heterogeneous cell populations. Specifically, we examined the transient slope of HEK-293 cells as a relatively homogeneous cell population [13] and hMSCs as a well-known heterogeneous cell population [16]. Next, we evaluated the transient slope of differentiated and undifferentiated hMSCs, as differentiation is known to produce more homogeneous cell populations. We then compared multiple cell populations with varying heterogeneity, including HEK-293 cells, cancer cells (PC3 and DU145), and hMSCs. Lastly, our focus on hMSCs was further expanded to include different tissue sources, bone-marrow (BM), adipose tissue (AT), and umbilical cord (UC) tissue-derived cells, as they are commonly used in transplantation studies. Transient slope was estimated using two methods: a linear trendline fitted to the low-frequency portion of the DEP spectrum, defined by 10 kHz–20 MHz (~13 data points) and 2 kHz–250 kHz (~17 data points). The number of data points illustrates the level of detail captured from the DEP spectrum for fitting the trendline and assessing transient slope. Transient slope and the standard deviation of transient slope were used as indicators of heterogeneity, based on the premise that more heterogeneous cell populations will have lower transient slope values and higher standard deviations. In contrast, more homogeneous cell populations will have higher transient slope values and lower standard deviations. To validate transient slope as a metric of heterogeneity, we assessed cell morphology, cell size, and cell stemness. We found that both methods for estimating transient slope yielded similar transient slopes, with the choice of method depending on intended application. Additionally, transient slope consistently tracked with the heterogeneity of all cell types investigated with hMSCs being most heterogeneous and HEK-293 cells being most homogeneous. This transient slope analysis provides a label-free metric of heterogeneity for critically important cell populations.

2. Materials and Methods

2.1. Cell Culture

All cells used in this study were obtained from the American Type Culture Collection (ATCC, Manassas, VA, USA). HEK-293 cells were cultured in Eagle's Minimum Essential Medium (Life Technologies, Carlsbad, CA, USA) supplemented with 10% fetal bovine serum (Corning, Corning, NY, USA). AT-hMSCs and UC-hMSCs were cultured in MSC basal media supplemented with 2% fetal bovine serum (ATCC), 5 ng/mL FGF-1 (ATCC), 5 ng/mL FGF-2, 5 ng/mL EGF (ATCC), and 0.1× antibiotic-antimycotic. BM-hMSCs were cultured in MSC basal media supplemented with 7% fetal bovine serum (ATCC), 15 ng/mL FGF-1, 125 pg/mL FGF-2, 2.4 mM L-alanyl-L-glutamine (ATCC), and 0.1× antibiotic-antimycotic. PC3 and DU145 cells were cultured in Roswell Park Memorial Institute (RPMI)-1640 media (Thermo Fisher, Waltham, MA, USA) supplemented with 10% (v/v) heat-inactivated fetal bovine serum (Corning), and 1% (v/v) penicillin-streptomycin (Fisher Scientific, Hanover Park, IL, USA). The cells were cultured at 37 °C in a humidified 5% CO_2 incubator using tissue culture-treated T-75 flasks, seeded at 5000 cells/cm^2, and passaged upon reaching ~80% confluency.

When passaging, the proliferation media was aspirated, the cell monolayer was rinsed using 1× DPBS (Life Technologies), and detached from the flask using 0.05% trypsin-ethylenediaminetetraacetic acid (Life Technologies) for 5 min at 37 °C. Once the cells were detached, the trypsin was neutralized with an equal volume of proliferation media. Then, the cells were pipetted into a 15 mL falcon tube, centrifuged at 275× g for 5 min, resuspended in new growth media, and counted using a hemacytometer for accurate seeding.

2.2. HMSC Differentiation

Tissue culture-treated 6-well plates were coated with 0.2% gelatin to prepare AT-hMSC for differentiation. The coating was prepared by dissolving lyophilized porcine skin gelatin (Sigma Aldrich, St. Louis, MO, USA) in Milli-Q water and autoclaving. Then, 900 µL of the gelatin solution was added to each well in the 6-well plate and allowed to coat at room

temperature for 30 min. The excess gelatin solution was aspirated, and the coated plates were placed in the biosafety cabinet to dry for at least 2 h.

AT-hMSCs were seeded at 10,000 cells/cm^2 in the gelatin-coated 6-well plate with growth media and allowed to proliferate for 2 days. For osteoblast differentiation, the growth media was aspirated, and the cells were rinsed once with 1× DPBS and the osteogenic medium was added, which consisted of αMEM (Life Technologies) supplemented with 10% fetal bovine serum, 50 µg/mL l-ascorbic acid 2-phosphate (FUJIFILM Wako, Osaka, Japan), 100 nM dexamethasone (MP Biomedicals, Santa Ana, CA, USA), 10 mM β-glycerophosphate (Alfa Aesar, Ward Hill, MA, USA), and 0.1× antibiotic-antimycotic. For adipocyte differentiation, the growth media was replaced with StemPro adipogenesis media (Life Technologies). The differentiation media was changed every 4 days for 21 days.

2.3. Transient Slope Characterization and Analysis

For the transient slope characterization, trypsinized cells were resuspended in a DEP buffer solution made of 8.5% (*w*/*v*) sucrose and 0.3% (*w*/*v*) glucose. The conductivity of the DEP buffer solution was adjusted to 100 µS/cm or 300 µS/cm with RPMI-1640. The cells were washed three times before final resuspension in the DEP buffer at 1×10^6 cells/mL. Cell viability was visually assessed using trypan blue. The prepared cells were then analyzed by the 3DEP analyzer (LabTech, Heathfield, UK), which features a microfluidic chip with 20 microwells containing 3-dimensional electrodes along with outer walls of the microwell. Two frequency ranges were investigated: 2 kHz–250 kHz and 10 kHz–20 MHz, at 10 V_{pp}. The resulting DEP spectrum reflected changes in light intensity as a function of frequency [17]. For quality control, each DEP spectrum underwent several checks. Initially, data obtained from each microwell of the 3DEP chip was visually screened for bubbles or insufficient power (visualized as smaller changes in light intensity). Data from affected microwells were excluded from the spectrum, and if four or more data points were excluded, the entire DEP spectrum was discarded. Next, each DEP spectrum obtained from a DEP run was compared to the 3DEP analyzer's built-in single-shell model to assess its shape. DEP runs with an R^2 value of 0.9 or higher when the model was fit to the experimental data were retained for further analysis. After this initial quality control screening, all of the DEP runs for a biological repeat (at least 10) were pooled together for a quartile test to identify outliers. No more than 4 outliers were removed per DEP run. If more than 4 outliers were identified, then the entire DEP run was no longer considered for the transient slope analysis. The transient slope of the DEP spectrum was determined by fitting a linear trendline to 20–80% of the rise time of the DEP spectrum with 80,000 cells tested per DEP run. Statistical analysis of transient slope was completed using one-way ANOVA with Tukey's post hoc test for multiple comparisons.

2.4. Cell Morphology and Size Analysis

At 80% confluency, each cell type was imaged at 10× magnification for cell morphology and size analysis. Morphology was assessed by examining the cells for characteristic shapes such as cobblestone, elongated, and spindle-like. Cell size was analyzed by quantifying cell area and diameter. For cells area measurements, images of cultured cells were processed in ImageJ version 1.80, where the scale bar on each image was measured and set for analysis. Utilizing the area measurement tool, at least 150 cells per cell type were selected and measured by outlining their perimeters. For cell diameter measurements, cells suspended in DEP buffer solution were imaged on a hemacytometer. The images were also processed in ImageJ, with the appropriate scale bar calibration. At least 100 cells per cell type were selected and measured by drawing a line across the width of each cell. Statistical analysis of cell areas and diameters was completed using one-way ANOVA with Tukey's post hoc test for multiple comparisons.

2.5. Cell Stemness Analysis with Immunostaining

Cells were seeded at a density of 1×10^4; cells per well in 48-well plate (Nunc Lab-Tek, Thermo Fisher Scientific) and cultured for 24–48 h until they reached 60–70% confluence. Then, cells were washed with phosphate-buffered saline (PBS) and fixed with 4% paraformaldehyde for 15 min at room temperature. After fixation, cells were washed three times with PBS and permeabilized using 0.1% Triton X-100 in PBS for 10 min at room temperature. To block nonspecific binding, cells were incubated in blocking buffer containing 5% bovine serum albumin in PBS for 30 min at room temperature.

Primary antibodies used to detect cell stemness included anti-SOX2 (rabbit polyclonal, 1:100, Abcam, Cambridge, United Kingdom) and anti-NANOG (mouse monoclonal, 1:200, Abcam). The AT-hMSCs, BM-hMSCs, UC-hMSCs, PC3 cells, and DU145 cells were individually incubated with each primary antibody diluted in blocking buffer overnight at 4 °C. Following incubation, the cells were washed three times with PBS, and incubated with Hoechst (Thermo Fisher) for 10 min at room temperature in the dark. Cells were washed three more times with PBS following Hoechst staining.

Immunofluorescence images were acquired using a Zeiss Axio Observer fluorescence microscope (Zeiss, Oberkochen, Germany) equipped with appropriate filters, capturing three fields per cell per antibody. These images were processed in ImageJ by conversion to an 8-bit scale, enhancing the green fluorescence signal using LookUp Tables (LUTs), and increasing brightness by 40–60% with corresponding contrast adjustments. Quantitative intensity analysis was performed to complement the visual assessment. Statistical analysis of cell areas and diameters was completed using one-way ANOVA with Tukey's post hoc test for multiple comparisons.

3. Results

3.1. Optimization of Transient Slope Obtained from DEP Spectra

This research required the execution of experiments that utilized the 3DEP analyzer [17]. Figure 1a depicts the DEP behavior of cells within the microwells (cells attracted towards walls display positive DEP, and cells repelled away from walls display negative DEP). Figure 1b provides a visual of a hypothetical DEP spectrum. Transient slope can be estimated from the spectrum by fitting a linear trendline to a wider (Figure 1c) and narrower (Figure 1d) frequency range, as demonstrated for a heterogeneous cell population (indicated by a schematic with red dashed box and red circles in hypothetical spectrum) and homogeneous cell population (represented by schematic with a blue dashed box and blue circles in hypothetical spectrum). We illustrate differences in the transient slope for homogeneous and heterogeneous cell populations with higher and lower values, respectively (Figure 1e).

Two methods were employed for transient slope data collection. In method 1, a wide frequency range (10 kHz–20 MHz) was tested, consistent with standard DEP experiments, and in method 2 a narrow frequency range (2 kHz–250 kHz) was tested. Figure 2 illustrates the efficiency of methods 1 and 2. Method 1 fitted an average of 13 data points to the transient slope trendline of the DEP spectrum (Figure 2a), and method 2 fitted an average of 17 data points to the transient slope trendline of the DEP spectrum (Figure 2b). The transient slopes from the two methods are plotted and compared in Figure 2c. The average transient slope was similar for both methods and the average R^2 value of the trendlines were similar (Figure 2d). This assessment was completed on a relatively homogenous cell population (Figure 2a–d) and a relatively heterogeneous cell population (Figure 2e–h). In this comparison, it can be seen that the average transient slope is higher in the homogeneous cell population independent of the method used and the R^2 values of the trendlines are high for both cell populations.

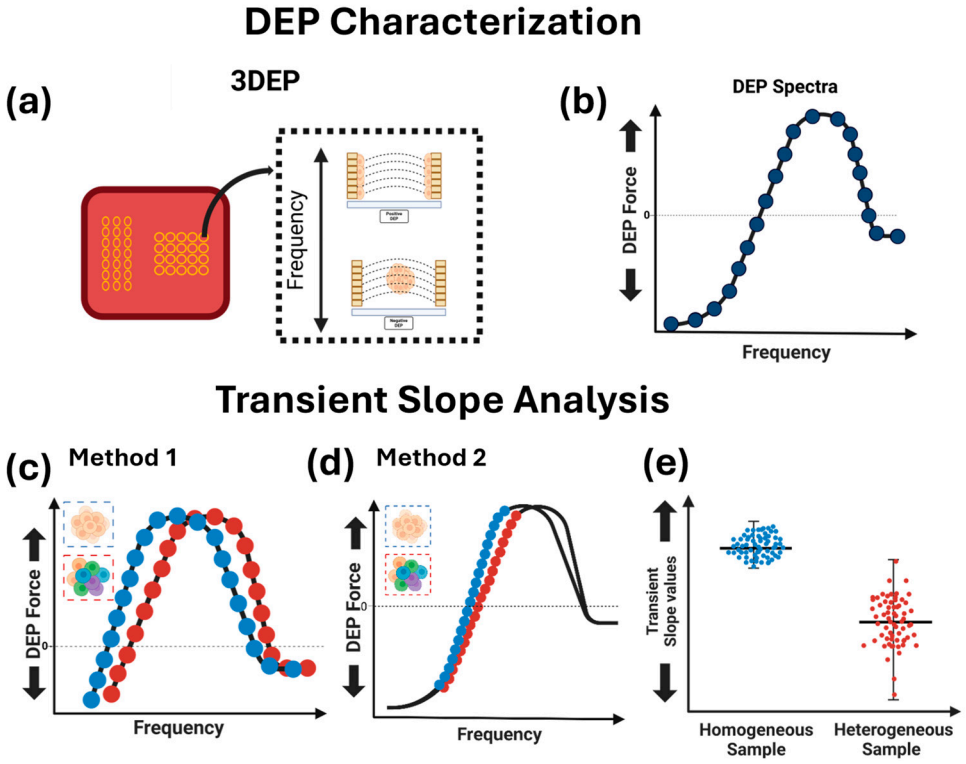

Figure 1. Schematic overview of transient slope analysis. (**a**) Cell polarization in dielectrophoresis (DEP) characterization of cells. The cells will either attract to areas of high electric field strength (positive DEP) or be repelled to areas of low electric field strength (negative DEP). (**b**) DEP spectrum generated from cell analysis. Two transient slope methods (**c**) sampling fewer data points and (**d**) sampling more data points. The blue circles and schematic outlined with blue dashed box represent hypothetical homogeneous cell population. The red circles and the schematic outlined with red dashed box represent hypothetical heterogeneous cell population. (**e**) Dot plot of transient slope of hypothetical homogeneous and heterogeneous cell populations. Homogeneous cell populations expected to have higher transient slope and heterogeneous cell populations expected to have lower transient slope. Note: this figure is a conceptual schematic and does not represent actual experimental data. Graphics in this figure were created with Biorender.com.

3.2. Transient Slope Assessments of Heterogenous and Homogenous Cell Populations

The transient slope was assessed for several cell populations that are classified as heterogeneous and homogeneous. As an initial assessment of the utility of transient as an indicator of cell heterogeneity, we examined undifferentiated and differentiated hMSCs. The hMSCs were differentiated toward osteoblasts and adipocytes (Figure 3). In this analysis, the average transient slope was highest for the differentiated hMSCs (osteoblast and adipocyte) and statistically different from that of the undifferentiated hMSCs (**** $p < 0.0001$), Figure 3a. A violin plot was utilized to emphasize the average and spread of transient slope for each cell population analyzed, illustrating a distinct distribution between differentiated and undifferentiated hMSCs, with the undifferentiated cells having the higher standard deviation (Figure 3b).

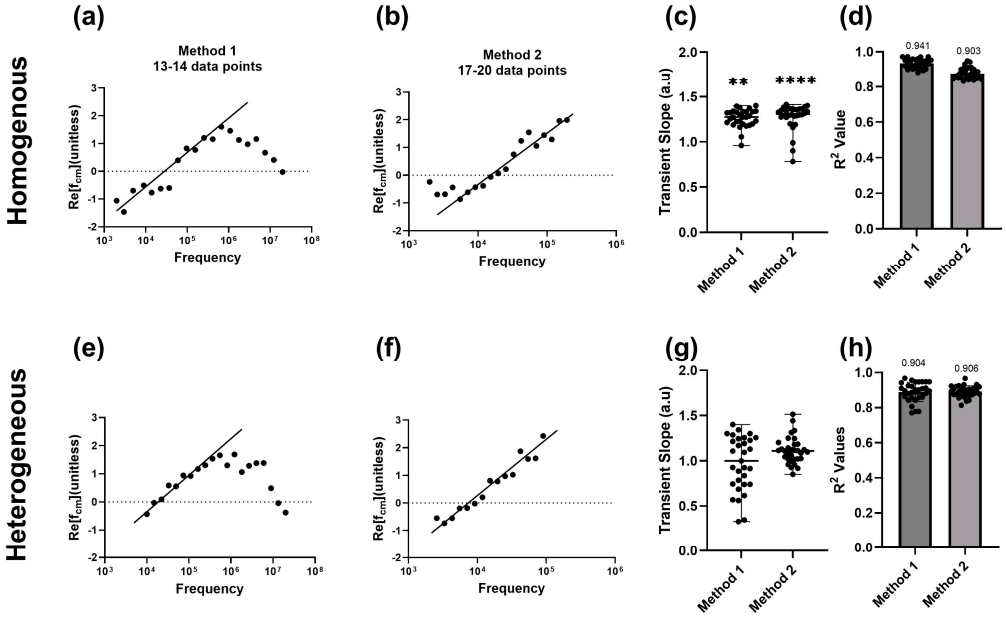

Figure 2. Comparison of two transient slope methods. (**a**,**e**) Method 1 transient slope trendline fitted to DEP spectrum defined by wide frequency range, 10 kHz–20 MHz. (**b**,**f**) Method 2 transient slope trendline fitted to DEP spectrum defined by narrow frequency range, 2 kHz–255 kHz. (**c**,**g**) Transient slopes and (**d**,**h**) trendline R^2 values for method 1 and method 2. (**a**–**d**) Depicts the collected data from a homogenous cell sample. (**e**–**h**) Depicts the data collected from a heterogeneous cell sample. The average R^2 value for method 1 and method 2 for the homogeneous cell sample is 0.941 and 0.903, respectively. The average R^2 value for method 1 and method 2 for the heterogeneous cell sample is 0.904 and 0.906, respectively. Error bars in (**c**,**g**) are standard deviation. For statistical significance: ** $p < 0.01$ and **** $p < 0.0001$.

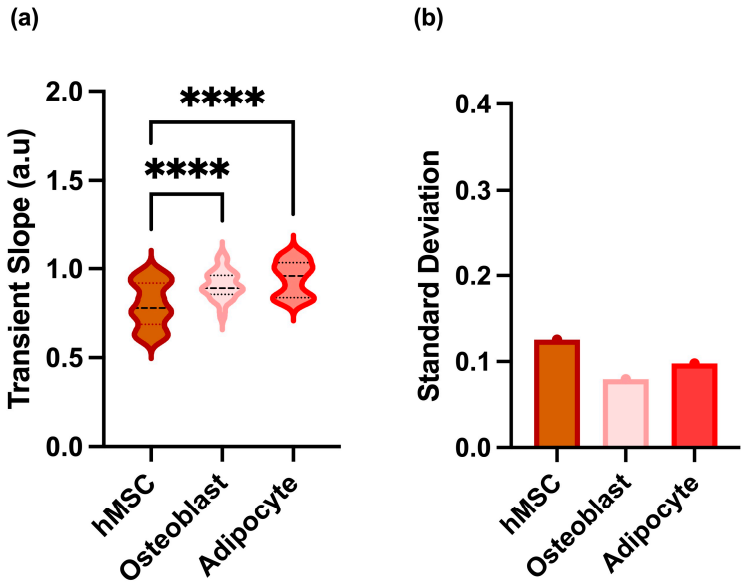

Figure 3. Transient slope of differentiated human mesenchymal stem cells (hMSCs). (**a**) Violin plot representation of transient slope. (**b**) Standard deviation of transient slopes. For statistical significance: **** $p < 0.0001$.

As a second assessment of the utility of transient slope as a measure of heterogeneity, we examined HEK-293, PC3, DU145, and AT-hMSCs. In Figure 4a, the average transient slope is highest for the HEK-293 cells and lowest for the hMSCs. A one-way ANOVA revealed that each cell population compared to the HEK-293 cells was different with

statistical significance (**** $p < 0.0001$). The violin plot shows distinct distributions with the HEK-293 cells having a wider top and tapered bottom, the PC3 cells having a tapered top and wider bottom, and the DU145 cells and AT-hMSCs having a more even distribution across the range of transient slopes. The standard deviation (or spread) of transient slopes was largest for the hMSCs and smallest for HEK-293 cells (Figure 4b). Supplementary Figure S1 illustrates how variability in transient slope for heterogeneous populations, such as hMSCs, may be attributed to differences in surface complexity.

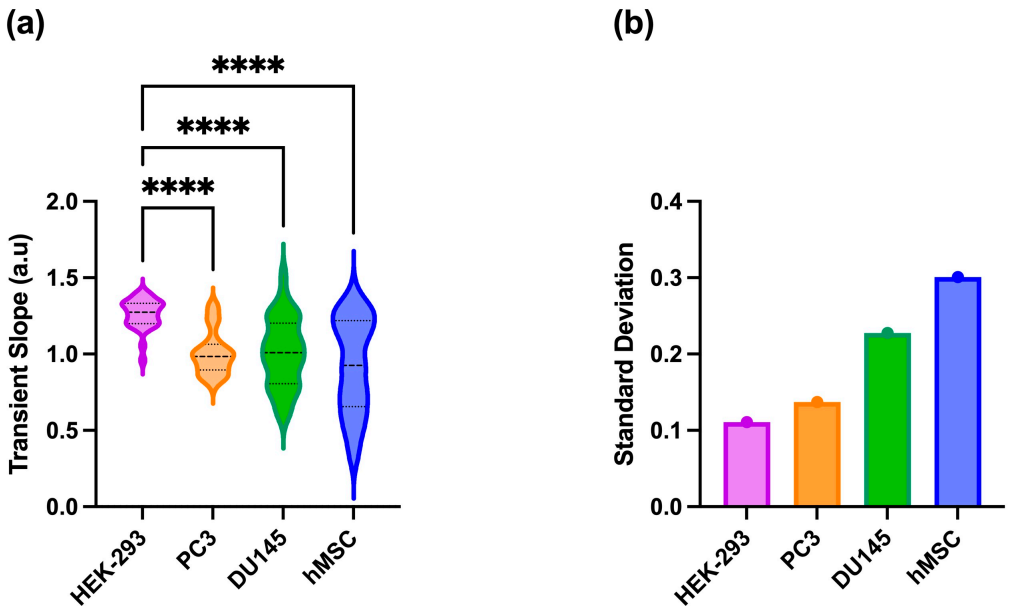

Figure 4. Transient slopes of HEK-293, PC3, DU145, and hMSCs. (**a**) Violin plot representation of transient slope. (**b**) Standard deviation of transient slopes. For statistical significance: **** $p < 0.0001$.

A cell area and cell diameter assessment was completed on the HEK-293, PC3, DU145, and hMSCs in ImageJ as a point of comparison for transient slope. Figure 5 shows cell culture images of all cells analyzed. The area of example cells is traced in yellow with an inset for better view. Visually, the HEK-293 cells and the DU145 cells looked similar in size (Figure 5a,b), with a cobblestone morphology. While the PC3 cells look similar in size to the HEK-293 cells and the DU145 cells, their morphology consisted of cobblestone and elongated cells (Figure 5c). The hMSCs had mostly elongated cells (Figure 5d). The cell area was tabulated and is represented as a violin plot in Figure 5e. The average cell area for the HEK-293 cells, DU145 cells, and PC3 cells was similar, while the average cell area for the hMSCs was higher. The average cell area of HEK-293 cells, DU145 cells, and PC3 cells was statistically significant in comparison to the hMSCs (**** $p < 0.0001$). Interestingly, the average of these cells, HEK-293, DU145, and PC3, was not statistically significant in comparison to each other. The violin plot illustrates a distinct distribution in cell area for the hMSCs, with this cell population having the highest standard deviation (Figure 5f). Supplementary Figure S2 presents the cell diameters of cells prepared for DEP analysis, which followed a similar trend to cell areas, though the differences between cell types were less pronounced. The hMSCs had the highest average diameter and largest standard deviation, while the HEK-293 cells had the lowest average diameter and the smallest standard deviation.

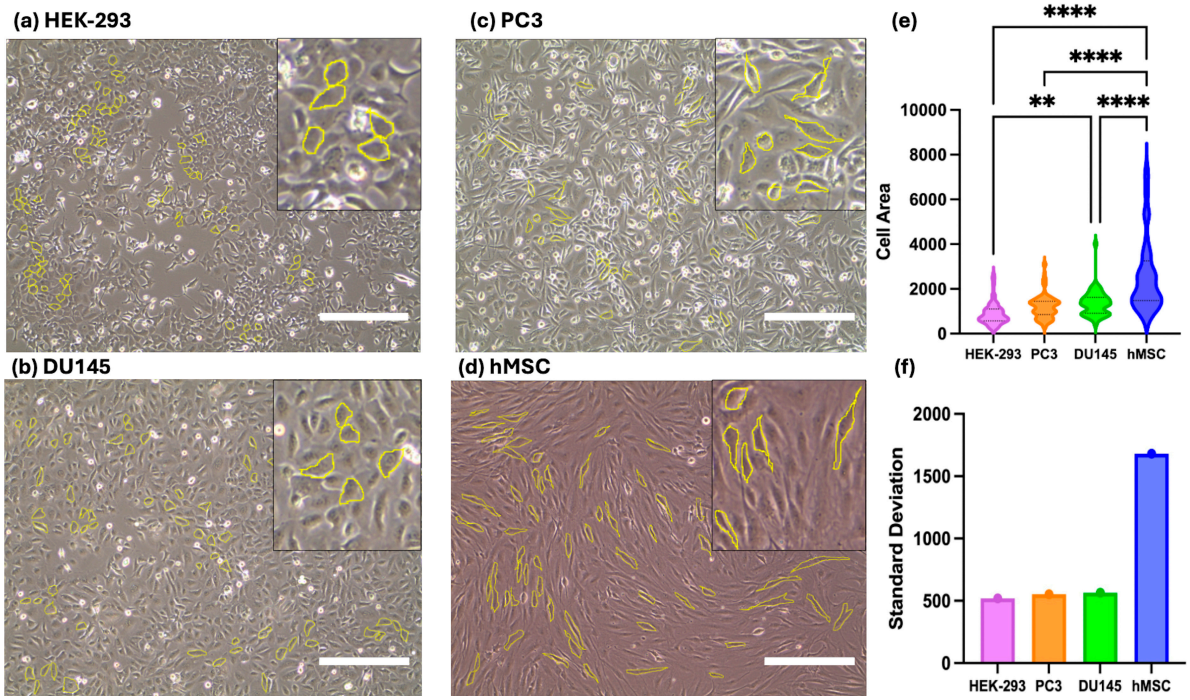

Figure 5. Cell area assessment of (**a**) HEK-293, (**b**) DU145, (**c**) PC3, and (**d**) hMSCs. (**e**) Violin plot of the cell area. (**f**) Standard deviation of the cell area. The scale bar is 400 µm. For statistical significance: ** $p < 0.01$ and **** $p < 0.0001$.

3.3. Effect of DEP Buffer Conductivity on Transient Slope

To further assess the efficacy of transient slope, we adjusted a key DEP experimental condition, buffer conductivity, and expanded the types of hMSCs analyzed. Figure 6 illustrates the transient slope of cancer cells (PC3 and DU145) and three different sources of hMSCs (AT, BM, and UC) measured at 300 µS/cm. The transient slope was highest for the cancer cells, with the BM-hMSCs having the lowest transient slope (Figure 6a). Compared to Figure 3, the distribution and spread of transient slope for the PC3 and DU145 cells is smaller. The PC3 and DU145 cells were statistically different from the BM-hMSCs (**** $p < 0.0001$) and UC-hMSCs (** $p < 0.01$ and * $p < 0.05$, respectively) while the AT-hMSCs and BM-hMSCs were statistically different (**** $p < 0.0001$) along with BM-hMSCs and UC-hMSCs (*** $p < 0.001$). There were distinct distributions, with the PC3 and DU145 cells having wider tops and tapered bottoms, and AT-, BM-, and UC-hMSCs having more even distribution across the range of transient slopes. PC3 and DU145 cells had smaller standard deviations than the hMSCs (Figure 6b).

3.4. Histogram Representation of Transient Slope

To identify the modality of transient slopes, histogram plots were generated. Figure 7 illustrates the histograms of all cell types we assessed. Each plot gives a Gaussian distribution, which shows how the transient slope data clusters around the mean value. Within the histograms, the Gaussian distribution formulates a bell curve over the area of the graph where the transient slope is most concentrated. The bins shown in each histogram plot indicate the frequency at which data points fell into those specific ranges. Figure 7a–c represents the transient slope of the HEK-293 (purple), PC3 (orange), and DU145 (green) cells. Figure 7d–f represents AT-hMSCs (blue), BM-hMSCs (dark blue), and UC-hMSCs (light blue). The bins represent the transient slope values (x-axis) while the DEP runs (y-axis) represent the number of technical replicates (~10 for each biological replicate) that yielded the binned transient slope value (synonymous to a frequency). The bins represent transient slope values for each experimental run with the various cell types. Figure 7a's largest bin was formulated from 7 data points with a range of 1.35 (±0.03). Each histogram plot is

defined by a unimodal Gaussian distribution of different widths reflective of the standard deviations. The three sources of hMSCs had larger widths in the Gaussian distribution than the HEK-293 cells, PC3 cells, and the DU145 cells.

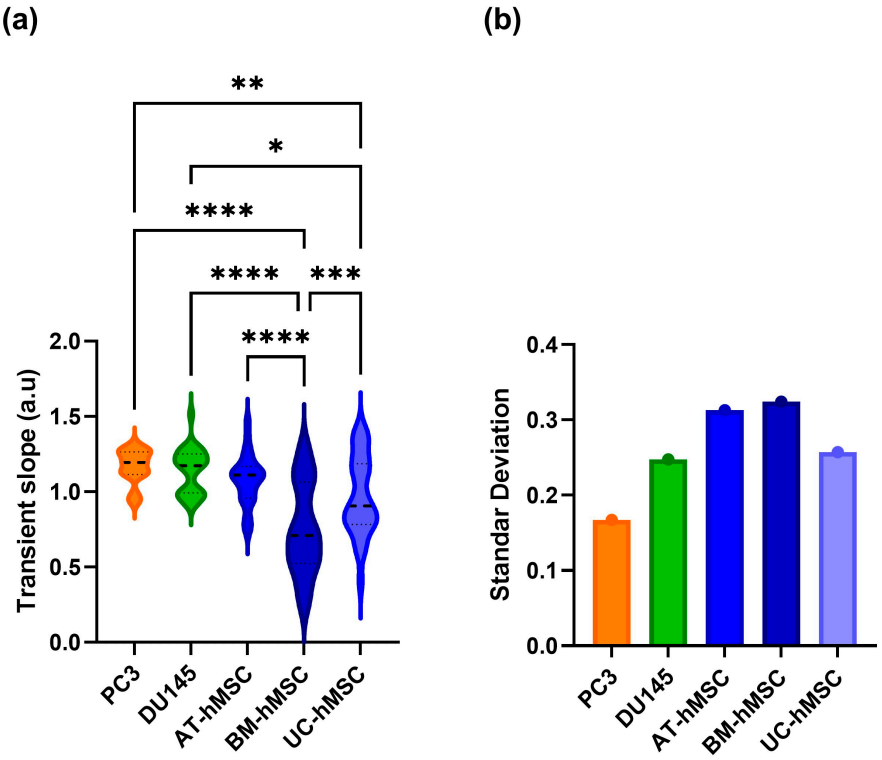

Figure 6. Transient slope of PC3, DU145, and AT-hMSCs, BM-hMSCs, and UC-hMSCs tested in a 300 µS/cm DEP buffer solution. (**a**) Violin plot representation of transient slope. (**b**) Standard deviation of transient slopes. For statistical significance: * $p < 0.05$, ** $p < 0.01$, *** $p < 0.001$, and **** $p < 0.0001$.

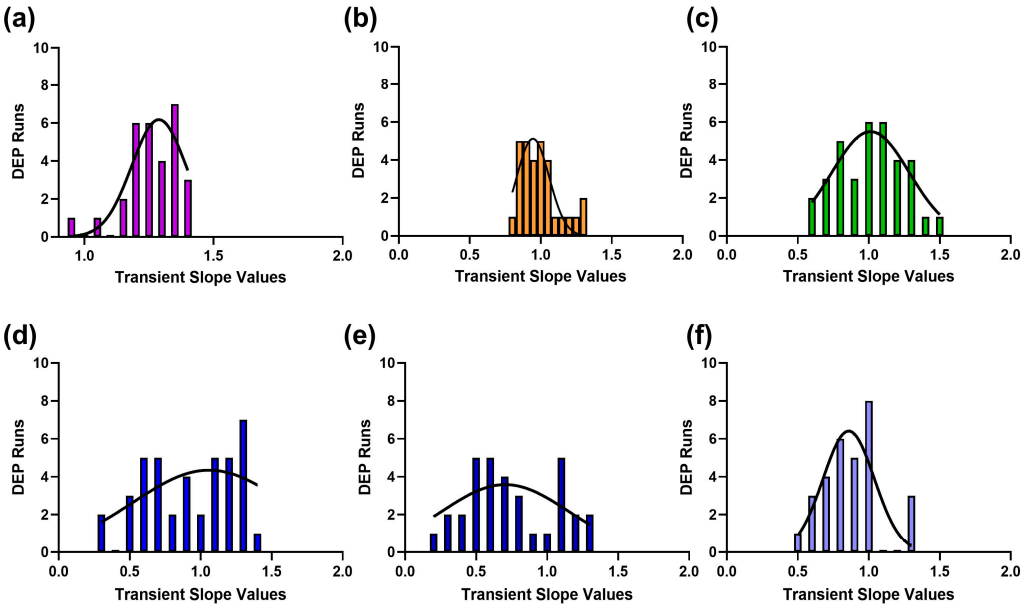

Figure 7. Histogram analysis of the transient slope of (**a**) HEK-293 cells, (**b**) PC3 cells, (**c**), DU145 cells, (**d**) AT-hMSCs, (**e**) BM-hMSCs, and (**f**) UC-hMSCs. A Gaussian distribution is plotted with the bins of transient slope values.

3.5. Stemness Marker Evaluation

Lastly, we assessed the cancer cells (PC3 and DU145) along with the hMSCs (AT, BM, and UC) for stemness as a biological indicator of heterogeneity. Figure 8 displays the protein expression of SOX2 and NANOG, two stemness markers for hMSCs and cancer cells, along with their quantification. Both cancer cell lines stained positive for SOX2 and NANOG, but their intensities were lower compared to the hMSCs. Among the hMSCs, UC-hMSCs exhibited the highest SOX2 intensity, while AT-hMSCs exhibited the highest NANOG intensity. The average intensity of SOX2 for PC3 and DU145 cells was statistically significant with comparison to the UC-hMSCs (* $p < 0.05$), while the average intensity of NANOG for DU145 cells and UC-hMSCs was statistically significant compared to the AT-hMSCs (* $p < 0.05$).

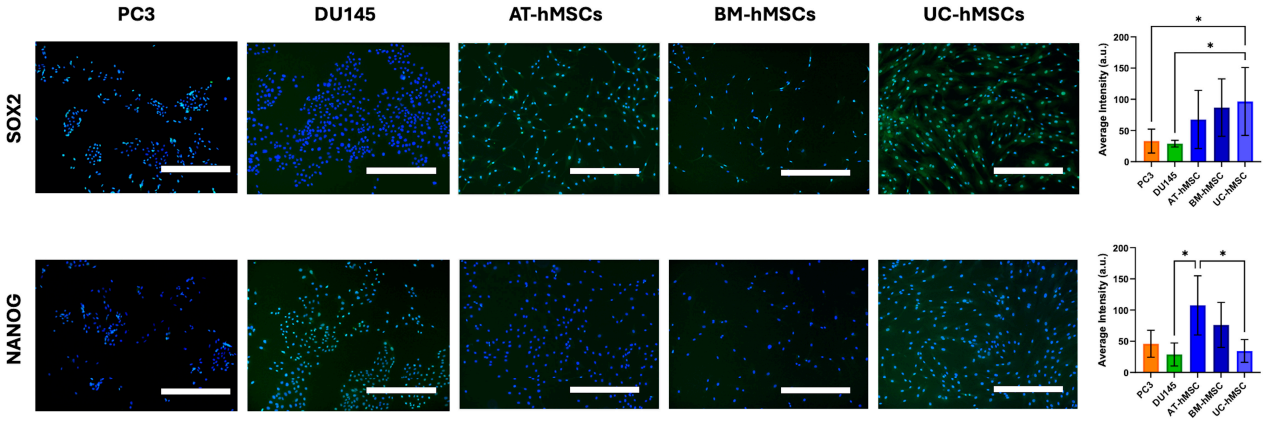

Figure 8. Stemness assessment of PC3 cells, DU145 cells, AT-hMSCs, BM-hMSCs, and UC-hMSCs. Immunofluorescent staining of SOX2 (top row) and NANOG (bottom row) with quantification. Images were processed for improved resolution, brightness, and contrast. The scale bar is 800 µm. For statistical significance: * $p < 0.05$.

4. Discussion

Assessing the heterogeneity of cell populations is essential to understand their basic functions. For instance, hMSCs are involved in various biological processes, including human development, immune response and disease progression [3]. Additionally, having a label-free marker of heterogeneity such as transient slope can be instrumental in developing electrokinetic based cell sorting strategies for cell biomanufacturing. Thus, we developed a methodology for estimating transient slope for a variety of cell populations. Since hMSCs are a well-known heterogeneous cell population [7], we compared them to differentiated hMSCs, suspected homogeneous cell populations HEK-293 cells, and cancer cells (PC3 and DU145 cells). HEK-293 cells were selected as a relatively homogeneous comparison population due to their well characterized DEP spectra [13], which remained consistent over several passages, reflecting their stability in cell culture [18]. PC3 and DU145 cells were chosen as comparison populations due to the presence of cancer stem-like cells [19], offering a contrasting population for assessing heterogeneity. DEP was chosen to measure transient slope because it provides a label-free workflow, enabling rapid cell analysis. Specifically, the 3DEP system allows for a full DEP spectrum to be generated for a cell population in just one hour. Additionally, in DEP, transient slope represents a measure of cells transitioning from negative DEP to positive DEP, providing insights into cell population heterogeneity.

We estimated transient slopes using methods 1 and 2 on relatively homogeneous HEK-293 cells and heterogeneous hMSCs. The homogeneous HEK-293 cells and heterogeneous hMSCs displayed typical DEP spectrum (Figure 2). Figure 2a,e illustrates that method 1 fitted ~13 data points to the transient slope trendline of the DEP spectra. Figure 2b,f illustrates that method 2 fitted ~17 data points to the transient slope trendline of the DEP

spectrum. Both methods overall yielded similar transient slopes, despite method 2 fitting to more data points (Figure 2c,g). For the heterogeneous hMSCs specifically, the transient slope obtained from method 2 was slightly higher than that from method 1, though the difference was not statistically significant. To maintain quality control of the transient slopes, we accepted only runs with an R^2 value of 0.9 or higher (Figure 2d,h). This analysis confirmed that both methods are valuable tools, and selection should be based on the intended application. Method 1 is ideal for obtaining a general DEP profile and transient slope of a cell population, as it provides data across the typical frequency range used in DEP analyses. In contrast, method 2, which samples a smaller frequency range, is more suitable for closely examining cell heterogeneity, particularly in suspected heterogeneous cell population. Lastly, the values of transient slope reflect underlying cell population characteristics with suspected homogeneous cell populations exhibiting higher slopes, as similar cell types within these populations transition more rapidly from negative DEP to positive DEP. Suspected heterogeneous cell populations show lower slopes, as the presence of subpopulations causes a slower transition from negative DEP to positive DEP.

To validate the utility of transient slope as an indicator of cell population heterogeneity, we analyzed (a) undifferentiated hMSCs alongside hMSCs differentiated toward osteoblasts and adipocytes, and (b) compared hMSCs to more homogeneous cell populations (HEK-293, PC3, and DU145 cells). When hMSCs undergo osteogenesis and adipogenesis, they differentiate into more specialized and a homogeneous cell populations. This is reflected in our transient slope results (Figure 3), where the average transient slopes of hMSCs differentiated into osteoblasts and adipocytes were higher compared to those of undifferentiated hMSCs, indicating the differentiated cells are more homogeneous than the undifferentiated hMSCs. In the second comparison, the average transient slopes of HEK-293, PC3, and DU145 cells were higher than those of hMSCs, confirming that hMSCs are more heterogeneous than these cell populations (Figure 4). The transient slope values of both cancer cell populations were similar, falling between those of HEK-293 and hMSCs, indicating the cancer cells had greater heterogeneity than the HEK-293 cells but less heterogeneity than the hMSCs.

These findings align with the known cell biology: HEK-293 cells are relatively homogeneous [20], hMSCs display high heterogeneity [7,21], and studies report the presence of cancer stem-like cells in PC3 and DU145 populations at levels of 0.2% [22] and 7–10% [23], respectively. Additionally, the violin plots and standard deviations support these findings. The spread of the transient slope data was greatest for the hMSCs and least for the differentiated hMSCs. This variability in transient slope for hMSCs may be influenced by differences in surface complexity, such as membrane proteins and glycosylation patterns (Supplementary Figure S1). To further substantiate our findings, we analyzed the cell size of HEK-293, PC3, DU145, and hMSCs (Figures 5 and S2). Visually, HEK-293 cells appeared uniform in size and shape, exhibiting an epithelial-like, polygonal morphology, while AT-hMSCs displayed more variation, with a spindle-like, elongated shape. Among these populations, hMSCs had the largest cell size with the greatest spread in cell area and diameter. The HEK-293 cells were the smallest; however, similar standard deviations were observed among HEK-293, PC3, and DU145 cells. Literature reports that cell size corresponds to the differentiation potential of hMSCs [24], which is indicative of heterogeneity.

A standard DEP buffer, 100 $\pm$ 5 μS/cm, was used to collect transient slope values shown in Figures 2–4. To determine if there were a dependency of transient slope on conductivity, we increased the DEP buffer conductivity to 300 $\pm$ 5 μS/cm (Figure 6). This is also relevant in developing electrokinetic cell sorting strategies, as buffer conductivity is a useful parameter to tune cell behavior [25,26]. We assessed cancer cells (PC3 and DU145 cells) and three sources of hMSCs (AT-, BM-, and UC-derived) and found that the increased buffer conductivity produced identical transient slope patterns to those obtained from our analyses with the 100 $\pm$ 5 μS/cm DEP buffer. Cancer cells were still less heterogenous than hMSCs, suggesting no dependency of transient slope on buffer conductivity within the range of 100 to 300 μS/cm. The histogram representation of transient slope for all cell

types examined (Figure 7) shows the number of DEP runs (i.e., technical replicates) that yielded each specific transient slope value. Cancer cells' Gaussian distribution peaked at transient slope value 1.0, where the DU145 cells had more variability than PC3 cells, as most values above 1.0 had a single DEP run. In contrast, the Gaussian distributions were flatter, and the peak varied for the hMSCs, further substantiating the use of transient slope as an indicator of cell population heterogeneity. Lastly, the phenotype assessment of cancer cells and hMSCs showed that the hMSCs (AT, BM, and UC) exhibited greater heterogeneity than the cancer cells based on stemness marker expression (Figure 8).

Overall, these results (Figures 2–8) support that transient slope reflects underlying cell population characteristics, with heterogeneous cell populations exhibiting lower slopes and homogeneous cell populations showing higher slopes.

Current methods for assessing cell population heterogeneity include flow cytometry, immunostaining, and various omics approaches (e.g., RNA sequencing, transcriptomics, proteomics). While these methods offer valuable insights into cellular characteristics, they often require predefined marker sets, extensive instrumentation, and significant sample preparation. For instance, flow cytometry and immunostaining are commonly used to assess protein expression in hMSCs but are limited by their dependency on a predetermined set of markers, which can vary across studies and may overlap with markers in other cell types [27,28]. In contrast, RNA sequencing does not require a predetermined set of markers, but it generates vast amounts of data that are resource-intensive to analyze and may still lack specificity in identifying functional heterogeneity within cell populations. Additionally, current methods tend to be time-consuming and costly, requiring substantial resources. Using transient slope as a heterogeneity metric offers a label-free, quantitative approach that simplifies sample comparisons and reduces variability associated with marker selection. Measuring transient slope with DEP also addresses limitations such as instrumentation size, lengthy processing times, and high costs, providing a versatile tool for assessing heterogeneity across various cell systems.

Some DEP studies have alluded to the importance of transient slope as a metric for distinguishing cell types or stem cell heterogeneity, but none have taken a systematic approach to demonstrate its utility. For example, Adams et al. [14] presented the idea of cell trapping curves derived from the DEP spectra, proposing that the slopes of these curves indicated cell population heterogeneity. This was applied to undifferentiated mouse neural stem and progenitor cells (mNSPCs) along with mNSPCs differentiated into astrocytes and neurons. While this methodology involved an additional processing step of converting the DEP spectra to a cell trapping curved based on the positive DEP behavior of cells, the estimated slopes corresponded with cell population heterogeneity. Similarly, we previously estimated transient slope from the DEP spectra of BM-hMSCs and AT-hMSCs, comparing them against a homogeneous control [13]. Our results demonstrated that transient slope effectively distinguished sources of hMSCs and reflected differences in heterogeneity. Collectively, these studies underscore the potential of transient slope from the DEP spectra as a label-free parameter of heterogeneity. Our study builds on this foundation by systematically establishing transient slope as an important heterogeneity metric by expanding on the parameter space explored. We extended the range of cell populations examined, varied buffer conductivity, and visualized transient slope distributions with histograms, comparing our findings with cell area and stemness assessments.

While our study has provided valuable insights into the validity of transient slope from the DEP spectrum for detecting cell population heterogeneity, it is important to note the limitations as opportunities for future research and enhancement. We validated transient slope on two clinically relevant cell systems, hMSCs stem cells and cancer cells, along with a relatively homogeneous cell population, HEK-293 cells. Although the average transient slope among these populations differed with statistical significance, incorporating a broader range of cell types, including a truly homogeneous control, would strengthen its validation. Such a control could be achieved using polystyrene beads, provided that buffer conductivity

can be tuned to allow the beads to display both negative and positive DEP behavior (typically, polystyrene beads exhibit negative DEP behavior at low conductivities [15]).

Single-cell measurements would further strengthen the use of transient slope as a metric of cell population heterogeneity. Quadrupole DEP devices will enable the characterization of transient slope of individual cells, while pseudo single-cell DEP measurements using the 3DEP system with low-density cell samples will provide an additional approach for single-cell assessment. Additionally, exploring nonlinear curve fitting techniques may yield more nuanced insights into transient slope and cell population heterogeneity.

Expanding the assays used to biologically confirm heterogeneity alongside transient slope measurements could enhance our findings. Enhancing cell morphology and area assessments through immunostaining with β-tubulin would offer structural insights. Similarly, broadening our stemness marker panel and integrating gene expression analyses would provide a more nuanced, quantitative assessment of cell heterogeneity.

Despite these limitations, our findings are significant. Studying cell population heterogeneity with transient slope offers a low cost, label-free metric that is not limited to the 3DEP system. Detecting heterogeneity is important for applications in cell characterization, cell differentiation, drug screening, cell biomanufacturing, and the study of human and disease development.

5. Conclusions

Transient slope values derived from the DEP spectrum are a promising label-free metric for assessing cell population heterogeneity. This study introduces important advancements, including the development of two methodologies for implementing transient slope, its application in characterizing the heterogeneity of stem cells and cancer cells, and a demonstration of its sensitivity in detecting heterogeneity. Integrating transient slope with existing methods for assessing cell population heterogeneity may facilitate the development of label-free cell sorting strategies, which are critical for downstream cell bioprocessing steps. Future investigations will focus on analyzing the transient slope of the high-frequency portion of the DEP spectra to further develop cell heterogeneity characterization. This will include DEP analysis, comprehensive cellular profiling to assess a broader range of stemness markers, and detailed morphological assessments. Ultimately, a label-free metric of cell population heterogeneity is essential to advancing our understanding of diverse cell systems.

Supplementary Materials: The following supporting information can be downloaded at: https://www.mdpi.com/article/10.3390/biophysica4040045/s1, Figure S1. Schematic representation of hypothetical subpopulations of cells with varying surface complexity [29–31]. Figure S2. (a) Diameter comparison of HEK-293 cells, PC3 cells, DU145 cells, and hMSCs. (b) Standard deviation of transient slopes.

Author Contributions: Conceptualization, E.E. and T.N.G.A.; methodology, E.E., T.W., Z.A.R., R.V. and T.N.G.A.; formal analysis, E.E.; investigation, E.E. and T.W.; resources, T.N.G.A.; data curation, E.E. and T.W.; writing—original draft preparation, E.E., T.W., Z.A.R. and T.N.G.A.; writing—review and editing, E.E., T.W., Z.A.R. and T.N.G.A.; supervision, T.N.G.A.; funding acquisition, T.N.G.A. All authors have read and agreed to the published version of the manuscript.

Funding: This research was funded by National Science Foundation, grant number 2048221.

Data Availability Statement: Data are contained within the article.

Conflicts of Interest: The authors declare no conflicts of interest.

References

1. Altschuler, S.J.; Wu, L.F. Cellular heterogeneity: Do differences make a difference? *Cell* **2010**, *141*, 559–563. [CrossRef] [PubMed]
2. Meacham, C.E.; Morrison, S.J. Tumour heterogeneity and cancer cell plasticity. *Nature* **2013**, *501*, 328–337. [CrossRef] [PubMed]
3. Nolan, D.J.; Ginsberg, M.; Israely, E.; Palikuqi, B.; Poulos, M.G.; James, D.; Ding, B.-S.; Schachterle, W.; Liu, Y.; Rosenwaks, Z. Molecular signatures of tissue-specific microvascular endothelial cell heterogeneity in organ maintenance and regeneration. *Dev. Cell* **2013**, *26*, 204–219. [CrossRef] [PubMed]

4. Hong, J.-H.; Hwang, E.S.; McManus, M.T.; Amsterdam, A.; Tian, Y.; Kalmukova, R.; Mueller, E.; Benjamin, T.; Spiegelman, B.M.; Sharp, P.A. TAZ, a transcriptional modulator of mesenchymal stem cell differentiation. *Science* **2005**, *309*, 1074–1078. [CrossRef]
5. Bruder, S.P.; Fink, D.J.; Caplan, A.I. Mesenchymal stem cells in bone development, bone repair, and skeletal regenaration therapy. *J. Cell. Biochem.* **1994**, *56*, 283–294. [CrossRef] [PubMed]
6. Singer, N.G.; Caplan, A.I. Mesenchymal stem cells: Mechanisms of inflammation. *Annu. Rev. Pathol. Mech. Dis.* **2011**, *6*, 457–478. [CrossRef] [PubMed]
7. Phinney, D.G. Functional heterogeneity of mesenchymal stem cells: Implications for cell therapy. *J. Cell. Biochem.* **2012**, *113*, 2806–2812. [CrossRef]
8. Pethig, R. Dielectrophoresis: Status of the theory, technology, and applications. *Biomicrofluidics* **2010**, *4*, 022811. [CrossRef] [PubMed]
9. Song, H.; Rosano, J.M.; Wang, Y.; Garson, C.J.; Prabhakarpandian, B.; Pant, K.; Klarmann, G.J.; Perantoni, A.; Alvarez, L.M.; Lai, E. Continuous-flow sorting of stem cells and differentiation products based on dielectrophoresis. *Lab Chip* **2015**, *15*, 1320–1328. [CrossRef]
10. Yoshioka, J.; Ohsugi, Y.; Yoshitomi, T.; Yasukawa, T.; Sasaki, N.; Yoshimoto, K. Label-free rapid separation and enrichment of bone marrow-derived mesenchymal stem cells from a heterogeneous cell mixture using a dielectrophoresis device. *Sensors* **2018**, *18*, 3007. [CrossRef]
11. Gascoyne, P.R.; Vykoukal, J. Particle separation by dielectrophoresis. *Electrophoresis* **2002**, *23*, 1973. [CrossRef]
12. Labeed, F.H.; Coley, H.M.; Hughes, M.P. Differences in the biophysical properties of membrane and cytoplasm of apoptotic cells revealed using dielectrophoresis. *Biochim. Biophys. Acta (BBA) Gen. Subj.* **2006**, *1760*, 922–929. [CrossRef]
13. Tsai, T.; Vyas, P.D.; Crowell, L.L.; Tran, M.; Ward, D.W.; Qin, Y.; Castro, A.; Adams, T.N.G. Electrical signature of heterogeneous human mesenchymal stem cells. *Electrophoresis* **2024**, *45*, 1562–1573. [CrossRef]
14. Adams, T.N.G.; Jiang, A.Y.L.; Vyas, P.D.; Flanagan, L.A. Separation of neural stem cells by whole cell membrane capacitance using dielectrophoresis. *Methods* **2018**, *133*, 91–103. [CrossRef] [PubMed]
15. Adams, T.N.G.; Leonard, K.M.; Minerick, A.R. Frequency sweep rate dependence on the dielectrophoretic response of polystyrene beads and red blood cells. *Biomicrofluidics* **2013**, *7*, 064114. [CrossRef] [PubMed]
16. Caplan, A.I.; Correa, D. The MSC: An injury drugstore. *Cell Stem Cell* **2011**, *9*, 11–15. [CrossRef]
17. Hübner, Y.; Hoettges, K.; Kass, G.; Ogin, S.; Hughes, M. Parallel measurements of drug actions on erythrocytes by dielectrophoresis, using a three-dimensional electrode design. In *IEE Proceedings-Nanobiotechnology*; IET: London, UK, 2005; pp. 150–154.
18. Zhang, L.; Gao, J.; Zhang, X.; Wang, X.; Wang, T.; Zhang, J. Current strategies for the development of high-yield HEK293 cell lines. *Biochem. Eng. J.* **2024**, *205*, 109279. [CrossRef]
19. Cruz, M.; Sidén, Å.; Calaf, G.; Delwar, Z.; Yakisich, J. The stemness phenotype model. *Int. Sch. Res. Not.* **2012**, *2012*, 392647. [CrossRef]
20. Pulix, M.; Lukashchuk, V.; Smith, D.C.; Dickson, A.J. Molecular characterization of HEK293 cells as emerging versatile cell factories. *Curr. Opin. Biotechnol.* **2021**, *71*, 18–24. [CrossRef]
21. Okamoto, T.; Aoyama, T.; Nakayama, T.; Nakamata, T.; Hosaka, T.; Nishijo, K.; Nakamura, T.; Kiyono, T.; Toguchida, J. Clonal heterogeneity in differentiation potential of immortalized human mesenchymal stem cells. *Biochem. Biophys. Res. Commun.* **2002**, *295*, 354–361. [CrossRef]
22. Rowehl, R.A.; Crawford, H.; Dufour, A.; Ju, J.; Botchkina, G.I. Genomic analysis of prostate cancer stem cells isolated from a highly metastatic cell line. *Cancer Genom. Proteom.* **2008**, *5*, 301–309.
23. Hurt, E.M.; Kawasaki, B.T.; Klarmann, G.J.; Thomas, S.B.; Farrar, W.L. CD44+ CD24− prostate cells are early cancer progenitor/stem cells that provide a model for patients with poor prognosis. *Br. J. Cancer* **2008**, *98*, 756–765. [CrossRef] [PubMed]
24. Haasters, F.; Prall, W.C.; Anz, D.; Bourquin, C.; Pautke, C.; Endres, S.; Mutschler, W.; Docheva, D.; Schieker, M. Morphological and immunocytochemical characteristics indicate the yield of early progenitors and represent a quality control for human mesenchymal stem cell culturing. *J. Anat.* **2009**, *214*, 759–767. [CrossRef] [PubMed]
25. Deivasigamani, R.; Mohd Maidin, N.N.; Abdul Nasir, N.S.; Abdulhameed, A.; Ahmad Kayani, A.B.; Mohamed, M.A.; Buyong, M.R. A correlation of conductivity medium and bioparticle viability on dielectrophoresis-based biomedical applications. *Electrophoresis* **2023**, *44*, 573–620. [CrossRef]
26. Markx, G.H.; Dyda, P.A.; Pethig, R. Dielectrophoretic separation of bacteria using a conductivity gradient. *J. Biotechnol.* **1996**, *51*, 175–180. [CrossRef] [PubMed]
27. Rojewski, M.T.; Weber, B.M.; Schrezenmeier, H. Phenotypic Characterization of Mesenchymal Stem Cells from Various Tissues. *Transfus. Med. Hemotherapy* **2008**, *35*, 168–184. [CrossRef] [PubMed]
28. Mebratie, D.Y.; Dagnaw, G.G. Review of immunohistochemistry techniques: Applications, current status, and future perspectives. *Semin. Diagn. Pathol.* **2024**, *41*, 154–160. [CrossRef] [PubMed]
29. Heiskanen, A.; Hirvonen, T.; Salo, H.; Impola, U.; Olonen, A.; Laitinen, A.; Tiitinen, S.; Natunen, S.; Aitio, O.; Miller-Podraza, H.; et al. Glycomics of bone marrow-derived mesenchymal stem cells can be used to evaluate their cellular differentiation stage. *Glycoconj. J.* **2008**, *26*, 367–384. [CrossRef] [PubMed]

30. Hamouda, H.; Ullah, M.; Berger, M.; Sittinger, M.; Tauber, R.; Ringe, J.; Blanchard, V. N-Glycosylation Profile of Undifferentiated and Adipogenically Differentiated Human Bone Marrow Mesenchymal Stem Cells: Towards a Next Generation of Stem Cell Markers. *Stem Cells Dev.* **2013**, *22*, 3100–3113. [CrossRef] [PubMed]
31. Yale, A.R.; Nourse, J.L.; Lee, K.R.; Ahmed, S.N.; Arulmoli, J.; Jiang, A.Y.; McDonnell, L.P.; Botten, G.A.; Lee, A.P.; Monuki, E.S.; et al. Cell Surface N-Glycans Influence Electrophysiological Properties and Fate Potential of Neural Stem Cells. *Stem Cell Rep.* **2018**, *11*, 869–882. [CrossRef] [PubMed]